

Revisiting the magnetic structure of Holmium at high pressure: a neutron diffraction study

M. Pardo-Sainz,^{1,2} F. Cova,¹ J. A. Rodríguez-Velamazán,³ I. Puente-Orench,¹ Y. Kousaka,⁴ M. Mito,^{5, a)} and J. Campo^{1, b)}

¹⁾*Instituto de Nanociencia y Materiales de Aragón (CSIC – Universidad de Zaragoza) and depto. de Física de la Materia Condensada, C/Pedro Cerbuna 12, 50009 Zaragoza, Spain.*

²⁾*Graduate School of Science, Osaka Metropolitan University, 1-1 Gakuencho, Sakai, Osaka 599-8531 Japan.*

³⁾*Institut Laue Langevin, 71 avenue des Martyrs, CS 20156, Grenoble, Cedex 9 38042, France.*

⁴⁾*Department of Physics and Electronics, Osaka Metropolitan University, 1-1 Gakuencho, Sakai, Osaka 599-8531 Japan.*

⁵⁾*Graduate School of Engineering, Kyushu Institute of Technology, Kitakyushu 804-8550, Japan.*

(Dated: 22 May 2023)

Low-temperature neutron diffraction experiments at $P = 8$ GPa have been conducted to investigate the magnetic structures of metallic Holmium at high pressures by employing a long d -spacing high-flux diffractometer and a Paris-Edinburgh press cell inside a cryostat. We find that at $P = 8$ GPa and $T = 5$ K, no nuclear symmetry change is observed, keeping therefore the hexagonal closed packed (hcp) symmetry at high pressure. Our neutron diffraction data confirm that the ferromagnetic state does not exist. The magnetic structure corresponding to the helimagnetic order, which survives down to 5 K, is fully described by the magnetic superspace group formalism. These results are consistent with those previously published using magnetization experiments.

I. INTRODUCTION

Ferromagnetic metals have played an important role in condensed matter physics from the viewpoint of its magnetism originated from itinerant electrons¹. In the $3d$ -electron ferromagnetic transition metals based on Fe, Co, and Ni, the mechanism responsible for their ferromagnetism can be understood within the Stoner model².

On the other hand, the ferromagnetism in the $4f$ -electron lanthanide metals, such as Gd, Tb, Dy, Ho, Er, and Tm, is explained by the Ruderman-Kasuya-Kittle-Yosida (RKKY) interaction between localized moments of the f -orbital electrons mediated by the conduction electrons³⁻⁵. The spatially damped oscillation of the conduction electron spin polarization is responsible of the competition between the ferromagnetic (FM) and anti-ferromagnetic (AFM) interactions, which often results in an incommensurate helimagnetic structure (HM).

At low temperatures, the subtle lattice contractions modify the RKKY interaction (J_{RKKY}) and the HM state is destabilized giving place to a FM ground state. Hereafter, the magnetic transition temperatures between the FM and HM states and between the HM and the paramagnetic (PM) states are denoted as T_C and T_N , respectively.

All $4f$ -lanthanide FM metals have an hexagonal closed

packed, hcp , structure with stacking unit ABA at ambient pressure (AP), and exhibit the structural series of transformations in the sequence hcp (ABA) \rightarrow Sm-type (ABABCBCACA) \rightarrow double- hcp ($dhcp$) (ABACA) \rightarrow fcc (ABCA) \rightarrow trigonal under increasing pressure.^{6,7}

The variation of the magnetic properties with the structural transformations in $4f$ -lanthanide metals has been studied theoretically⁸ and reported experimentally by magnetic characterization⁹⁻¹³, electrical resistivity¹⁴⁻²⁰, neutron diffraction^{14,16,21-25}, X-ray diffraction²⁶, and Mössbauer spectroscopy²⁷. In particular, neutron diffraction experiments have been successfully employed to study the magnetic phases of Ho metal at high pressures and variable temperatures, as we briefly summarize in the next paragraph.

The first neutron scattering experiment in this metal was performed at AP by Koehler *et al.*²⁸. In it, they reported that the Ho magnetic moments form a basal plane helix below $T_N = 133$ K, and a conical configuration was developed below $T_C = 20$ K, with a net magnetic moment parallel to the c -axis, in agreement with later neutron experiments^{29,30}. In year 1968, Umeyayashi *et al.*²¹ studied Tb and Ho at pressures below 1 GPa and temperatures above 80 K, where the pressure dependences of T_N and the helical turn angle were measured. It was found that the HM ordering occurs at lower temperatures with increasing pressure. In 1988, Achiwa *et al.*³¹ studied the Ho metal up to 2.1 GPa in the temperature range 10 K to T_N . The helical pitch angle evolution with temperature was found in agreement with Ref.²¹ for $P = 0.6$ GPa, while for higher pressures the values of the angle increased, and a lock-in value appeared below 20 K.

^{a)}Electronic mail: mitoh@mns.kyutech.ac.jp

^{b)}Electronic mail: javier.campo@csic.es

Recently, the new available extreme conditions neutron diffractometers have facilitated the study of the high pressure region of Holmium. In 2012, Thomas *et al.*¹⁴ performed neutron diffraction experiments at maximum pressures of 6.6 GPa at 89, 110 and 300 K. They established the incommensurate nature of the HM phase and determined the decrease of T_N from approximately 122 K at AP at a rate of -4.9 K/GPa up to a pressure of 9 GPa, above which the PM to HM transition vanishes, in agreement with Ref.^{21,31}. In 2020, Perreault *et al.*²⁵ performed neutron diffraction experiments at maximum pressures of 20 GPa and minimum temperatures of 10 K. They observed two magnetic transitions below 10 GPa: one to an incommensurate HM phase and another to a conical FM phase. For pressures above 10 GPa in the Sm-type phase, and above 19 GPa in the *dhcp* phase, the appearance of a magnetic peak at 3 Å and the increase of the intensity of some nuclear peaks were assigned to the presence of a FM ordering below 30 K.

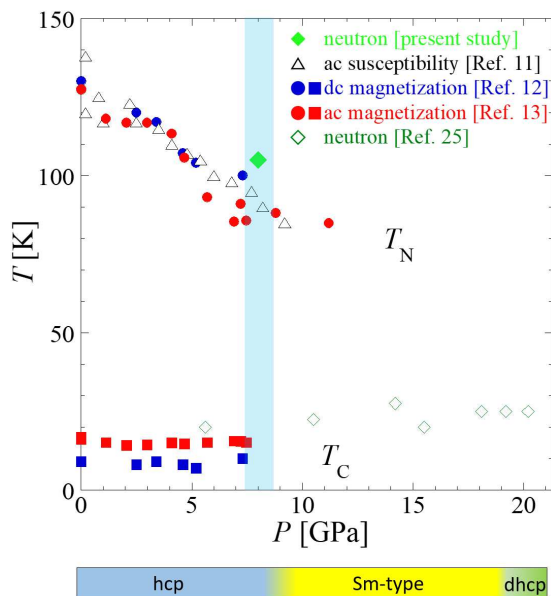


FIG. 1. (Colour online) P dependence of T_N and T_C for Ho¹¹⁻¹³. The green point at $P = 8$ GPa and $T_N = 105$ K has been determined in this study. Blue and red symbols correspond to the data obtained from our previous magnetic characterization studies using an SQUID magnetometer, while the black empty triangles and green empty diamonds correspond to the previous a.c. susceptibility and neutron diffraction experiments, respectively. The size of the error bars, in temperature and pressure, is smaller than the size of the symbols employed. The color bar at the bottom part of the figure indicates the different phase transformations happening as the pressure increases at room temperature according to ref.³². The present study focuses on the light-blue shaded region.

The P dependence of T_N and T_C , evaluated with magnetic susceptibility¹¹ (black-empty symbols), a.c and d.c magnetization^{12,13} (blue and red filled symbols), and neutron diffraction²⁵ (green-empty symbols) is showed

for Ho in the magnetic phase diagram in Fig. 1.

In our recent a.c. magnetization measurements, using a superconducting quantum interference device (SQUID) magnetometer at zero applied magnetic field ($H_{dc} = 0$ T), the signal of the FM anomaly was reduced below any detectable level at a pressure between 5.7 and 8.8 GPa¹³. The anomaly at 5.7 GPa suggested a first order phase transition that remained in the range 0.5 - 11.6 GPa after remeasuring the sample by decreasing the pressure from 11.2 GPa (the results in the sequence after 11.2 GPa are not visible in Fig. 1 but details can be found in ref.¹³). Thus, residual strain influenced the suppression of the FM order.

In our previous d.c. magnetization measurements at $H_{dc} = 0.5$ T, which is one-third of the critical field to the saturated state, the FM anomaly was still observed at 7.3 GPa, and a broad hump appeared at 9.2 GPa¹². It suggests that the FM order becomes unstable above 7.3 GPa and a short range order composed of small grains is developed at 9.2 GPa. In different magnetization measurements, using a SQUID vibrating-coil-magnetometer method, the development of a ferromagnetic magnetization was observed at 8.2 GPa, which disappeared at 12 GPa¹³. All these facts together stressed that the P region of 8 - 12 GPa is a critical region for the FM ordering.

Thus, different series of magnetic measurements showed that; i) the HM transition was observed at pressures up to 12 GPa, while the FM transition seems to be unstable at approximately 8 GPa, and ii) the ferromagnetic short range ordering could survive until approximately 11 GPa^{12,13}.

However, previous neutron diffraction experiments, covering a d spacing between 1.0 - 3.5 Å, reported that the FM ordering survives until at least 20 GPa²⁵. Therefore, it seems that a controversy exists between the last neutron diffraction experiments by Perreault *et al.*²⁵ and the macroscopic magnetic characterization of Ho at high pressures^{12,13}.

To solve this controversy, in the present study, by performing neutron powder diffraction experiments at low temperatures, but covering a wide d -spacing region ($1.4 \leq d \leq 50$ Å), we determined the magnetic structure at 8 GPa, in the temperature range $5 \leq T \leq 300$ K. The magnetic superspace group (MSSG) formalism³³⁻³⁵ has been employed to classify the symmetry of the magnetic structure.

II. HIGH PRESSURE NEUTRON DIFFRACTION EXPERIMENTS

Polycrystalline sample of metallic natural Ho with high purity (99.999%) was purchased from Sigma-Aldrich. Especial care was taken to manipulate the sample minimizing the exposure time to air.

Neutron powder diffraction experiments were carried out on the high-flux 2-axis neutron diffractometer D1B of the Institut Laue-Langevin (ILL) in Grenoble, France.

This instrument has a MWGC 1D-detector spanning an angular range of 128° with a definition of 0.1° . A Radial Oscillating Collimator (ROC) was installed in order to eliminate the spurious signals produced by the sample environment.

Two data acquisitions were taken at AP and room temperature (RT) for a Ho powder sample inside a 6 mm diameter vanadium can, with neutron wavelengths of $\lambda = 1.28 \text{ \AA}$ and 2.52 \AA which allowed to explore d -spacings, respectively, of $0.7\text{--}15.0 \text{ \AA}$ and $1.4\text{--}50 \text{ \AA}$.

The data collection at 8 GPa were performed with $\lambda = 2.52 \text{ \AA}$ which correspond to the maximum flux configuration of the D1B instrument. For these acquisitions, the powder was placed in a null-scattering TiZr gasket using a deuterated 4:1 ethanol-methanol mix as pressure transmitter medium, (the same that the one employed before by Perreault *et al.* at 20 GPa²⁵), which is the typical in all the neutron diffraction experiments. Then, it was introduced inside a VX5/180 Paris-Edinburgh (PE) pressure cell^{36,37} equipped with SINE-type sintered diamond anvils³⁸. A pressure of 0.12 GPa was applied to the PE cell, which for the sample corresponded to 8 GPa, after calibration with a Pb flake placed with the sample. Then the PE cell was cooled using liquid nitrogen and helium from RT to 5 K. At this temperature, a 4.5 hours isotherm acquisition was performed. Then the sample was warmed back to RT in 10 hours and diffractograms were collected every 15 minutes.

It is well known that the 4:1 ethanol-methanol mixture is not the *ideal* transmitting media at low temperatures but it is a good approach to the hydrostatic behavior at room temperature for pressures below 10 GPa³⁹. Furthermore, the fact that we do not detect any remarkable change, with decreasing the temperature, with the sample inside the PE cell, neither in the background of the diffractograms, nor in the width of the Bragg lines (see Fig. 3), suggests that the quality of the pressure at 5 K is good enough in our experimental conditions.

Different crystallographic tools were employed for the determination of the crystal and magnetic structures, which include the FullProf Suite⁴⁰, the ISODISTORT Suite^{41,42}, and utilities within the Bilbao Crystallographic Server^{43–46} for the symmetry analysis and visualization.

III. RESULTS AND ANALYSIS

A. $P = 0 \text{ GPa}$

Figure 2 shows the diffraction patterns collected with wavelengths $\lambda = 1.28 \text{ \AA}$ (top) and 2.52 \AA (bottom). The peaks observed in the diffraction patterns at AP and RT can be indexed by the paramagnetic $P6_3/mmc.1'$ MSSG (No. 194.264). This crystal structure corresponds with a *hcp* structure where the Ho atom is located in the Wyckoff position (WP) $2c$, with coordinates $(1/3, 2/3, 1/4)$. The cell parameters obtained from a multi-

pattern refinement of both diffractograms are: $a = b = 3.5690(2) \text{ \AA}$, $c = 5.6020(4) \text{ \AA}$, $\alpha = \beta = 90^\circ$, $\gamma = 120^\circ$; with $R_{\text{Bragg}} = 15.1$ and 11.2 , for $\lambda = 1.28 \text{ \AA}$ and 2.52 \AA , respectively.

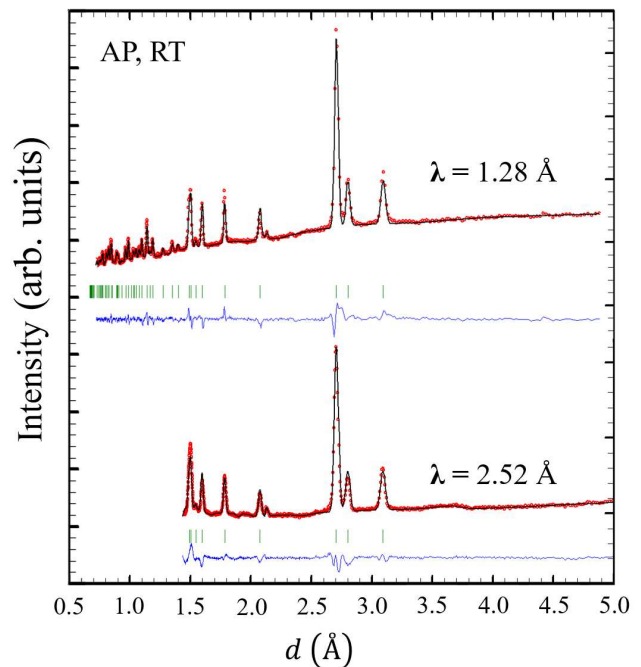


FIG. 2. (Colour online) Diffraction patterns collected with $\lambda = 1.28 \text{ \AA}$ (up) and 2.52 \AA (down) at RT and AP. In red are shown the observed points and in black continuous line the calculated pattern with the parameters described in the main text. The blue continuous line and the green ticks indicate, the difference between the observed and calculated profile, and the nuclear peaks generated by the space group, respectively.

B. $P = 8 \text{ GPa}$

Insert of Fig. 3 shows the diffraction pattern collected with $\lambda = 2.52 \text{ \AA}$ at $P = 8 \text{ GPa}$ and $T = 5 \text{ K}$. The first remarkable fact is the presence of a new high-intensity peak observed at $d \sim 21 \text{ \AA}$ that was not present in the diffractograms taken at RT. The low part of the Fig. 3 shows a zoom of the small d -spacing region for the diffractograms collected at $T = 5 \text{ K}$ (middle part) and RT (bottom part) with the sample inside the PE cell in the cryostat. With this complex sample environment, once the sample is inside the gasket in the PE cell, the intensity is greatly suppressed, and a huge increase of the background is observed, even with the ROC in front of the detector. This is expected since for high pressure experiments, the quantity of sample irradiated by the neutron beam is much smaller.

The diffractogram observed at RT inside the PE cell,

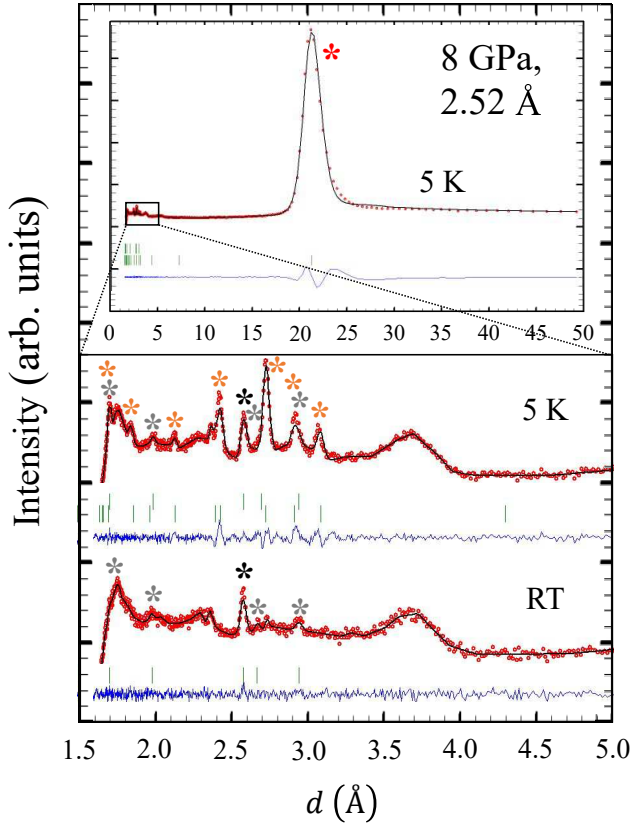


FIG. 3. (Colour online). The insert shows the 5 K diffractogram in the full d -spacing scale accessible with the neutron wavelength $\lambda = 2.52 \text{ \AA}$ at 8 GPa. A large magnetic signal appears at $\sim 21 \text{ \AA}$. A zoom of the small d -spacing region of the diffractograms collected with $\lambda = 2.52 \text{ \AA}$ is displayed in the middle part (5K) and bottom part (RT) of the figure. In red are shown the observed points and in back continuous line the calculated pattern with the parameters described in the main text. The blue continuous line and the green ticks indicate the difference between the observed and calculated profile and the nuclear and satellite peaks generated by the magnetic superspace group, respectively. Red and orange asterisks label the satellite peaks visible only in the HM phase. Black and grey asterisks label the nuclear peaks visible at both temperatures. The broad feature around 3.7 \AA and the small peak at $\sim 2.3 \text{ \AA}$ are due to the pressure transmitting fluid and the Pb flake, respectively, and treated as background contributions.

after warming from 5K, is indexed by the same hcp structure ($P6_3/mmc.1'$) with shorter cell parameters ($a = b = 3.4030(7) \text{ \AA}$, $c = 5.345(2) \text{ \AA}$, and $R_{\text{Bragg}} = 6.07$) that the one observed at AP. Therefore, no structural transition to the Sm-type phase has been observed as the pressure was increased from AP to 8 GPa.

However, at 8 GPa and 5 K, several new magnetic satellites appear, marked with red and orange asterisks in Fig. 3, including the one clearly observed at $d \sim 21 \text{ \AA}$. These satellites are indexed with an incommensurate propagation vector $\vec{k}_{\text{HM}} = (00\delta)$ with $\delta = \pm 0.2536(1)$, in units of c^* , in agreement with Ref.²⁵. The plus or minus

sign in the propagation vector indicates a clock-wise or anti clock-wise propagation. The nuclear peaks, marked with black and grey asterisks in Fig. 3, remain unchanged respect to the ones at RT, suggesting that no FM order is present, even at the lowest temperature. The analysis of this new magnetic state will be elucidated in the next subsection.

1. Symmetry analysis

We use the symmetry analysis to reduce the number of possible magnetic ground states in Ho- hcp compatible with the observed propagation vector \vec{k}_{HM} . We can decompose the magnetic representation for the Ho atom, located at WP $2c$, as a direct sum of Irreducible Representations (*irreps*) of the parent group $P6_3/mmc.1'$ for the Δ point, (00δ) , of the Brillouin zone (BZ)⁴⁷, as follows:

$$m\Gamma_{2c} = 1m\Delta_2(1) \oplus 1m\Delta_3(1) \oplus 1m\Delta_5(2) \oplus 1m\Delta_6(2).$$

The basis vectors of each *irrep* are given in Table I. The magnetic structure described by both, the 1d-*irreps* $m\Delta_2$ and $m\Delta_3$ consists of a sinusoidal modulation along the c -axis. Meanwhile, the 2d-*irreps*, $m\Delta_5$ and $m\Delta_6$, describe helices in which the magnetic moments are contained in ferromagnetic ab planes, and propagate along the c -axis. However, both models differ greatly when considering the phase-shift between the Ho atoms in the unit cell. While in the case of $m\Delta_6$ the phase-shift is the same as the pitch angle of the helix: $\phi = 180 \times k_{\text{HM}} = \pm 45.65(2)^\circ$, in $m\Delta_5$ the phase-shift is given by: $\phi = 180 \times (k_{\text{HM}} + 1) = \pm 225.65(2)^\circ$. Therefore, the magnetic structure given by $m\Delta_6$ can be considered as a single helix, while for $m\Delta_5$ the system is composed of two independent helices, one for each atom in the unit cell. The magnetic structure at 5 K, labelled with $m\Delta_6$, and the ϕ angle are depicted in Fig. 4.

TABLE I. Basis vectors (BV) of each *irrep* present in the magnetic representation of the Ho $2c$ site for the space group $P6_3/mmc.1'$ with $\vec{k}_{\text{HM}} = (00\delta)$. The basis vectors components are expressed in terms of the crystallographic axis a , b and c .

<i>irrep</i>	BV	Ho 1 (1/3 2/3 1/4)	Ho 2 (2/3 1/3 3/4)
$m\Delta_2$	ψ_1^2	(001)	(001) $e^{-i\pi\delta}$
$m\Delta_3$	ψ_1^3	(001)	(00 $\bar{1}$) $e^{-i\pi\delta}$
$m\Delta_5$	ψ_1^5	$\left(1 - \frac{1}{\sqrt{3}}i, -\frac{2}{\sqrt{3}}i, 0\right)$	$\left(1 - \frac{1}{\sqrt{3}}i, -\frac{2}{\sqrt{3}}i, 0\right) e^{-i\pi(\delta+1)}$
	ψ_2^5	$\left(-\frac{2}{\sqrt{3}}i, 1 - \frac{1}{\sqrt{3}}i, 0\right)$	$\left(-\frac{2}{\sqrt{3}}i, 1 - \frac{1}{\sqrt{3}}i, 0\right) e^{-i\pi(\delta+1)}$
$m\Delta_6$	ψ_1^6	$\left(1 - \frac{1}{\sqrt{3}}i, -\frac{2}{\sqrt{3}}i, 0\right)$	$\left(1 - \frac{1}{\sqrt{3}}i, -\frac{2}{\sqrt{3}}i, 0\right) e^{-i\pi\delta}$
	ψ_2^6	$\left(-\frac{2}{\sqrt{3}}i, 1 - \frac{1}{\sqrt{3}}i, 0\right)$	$\left(-\frac{2}{\sqrt{3}}i, 1 - \frac{1}{\sqrt{3}}i, 0\right) e^{-i\pi\delta}$

After a systematic trial and error procedure, it was observed that $m\Delta_2$, $m\Delta_3$ and $m\Delta_5$ do not fit the data,

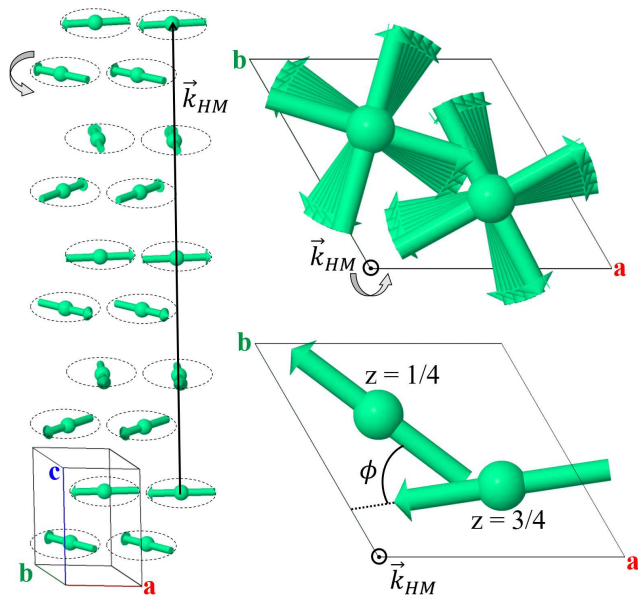


FIG. 4. (Colour online) Magnetic structure obtained from the refinement of the data with the model given by the $P6_322.1'(00\gamma)h00s$ MSSG. Five nuclear unit cells along c axis are shown. The right bottom side shows the pitch angle ϕ formed by the magnetic moments in adjacent ferromagnetic ab planes along c . The right upper side shows a projection of the magnetic moments onto the ab planes.

since they assign zero intensity for the main magnetic peak indexed as $(000) \pm \vec{k}_{\text{HM}}$ at $d \sim 21$ Å. However, the magnetic satellite reflections (red and orange asterisks in Fig. 3) can be correctly fitted by the 2d-*irrep* $m\Delta_6$.

The combination between the parent group $P6_3/mmc.1'$ and the magnetic modulations for Ho atoms given by the *irrep* $m\Delta_6$ give as a result the $P6_322.1'(00\gamma)h00s$ MSSG. Within the MSSG formalism, the magnetic structure is described by a basic structure, related to the nuclear paramagnetic cell, in addition to a series of magnetic modulation functions that describe the variation from the basic structure of the magnetic moments. In our case, with just one propagation vector \vec{k}_{HM} and no net magnetic moment (i.e. no existence of a propagation vector $\vec{k}_{\text{FM}} = (000)$), the magnetic structure is described by:

$$\vec{M}_{lj} = \vec{M}_{j,s} \sin(2\pi x_4) + \vec{M}_{j,c} \cos(2\pi x_4),$$

where the internal coordinate x_4 is given by the product of the propagation vector and the position \vec{r}_{lj} of the atom j in the l -th unit cell ($x_4 = \vec{k}_{\text{HM}} \cdot \vec{r}_{lj}$).

The explicit amplitudes of the cosine ($\vec{M}_{j,c}$) and sine ($\vec{M}_{j,s}$) components of the magnetic moment for the $P6_322.1'(00\gamma)h00s$ MSSG are given in Table II. In this MSSG, the Ho atom remains in the WP $2c$ position and the symmetry constraints imposed allow only for 1 free parameter to describe the magnetic structure, which is

the modulus of the magnetic moment (M).

TABLE II. Structural and magnetic parameters for Ho metallic at 8 GPa and $T = 300$ and 5 K obtained from the analysis of the patterns collected at D1B. The cosine ($\vec{M}_{j,c}$) and sine ($\vec{M}_{j,s}$) components of the magnetic moment are expressed in terms of the crystallographic axis a , b and c .

Phase T (K)	PM 300	HM 5
MSSG	$P6_3/mmc.1'$	$P6_322.1'(00\gamma)h00s$
#	194.264	182.1.24.2.m180.2
\vec{k}		(00δ)
δ		0.2536(1)
ϕ ($^\circ$)		45.65(2)
<i>irrep</i>		$m\Delta_6$
a (Å)	3.4030(7)	3.3976(6)
c (Å)	5.345(2)	5.390(1)
c/a	1.5707(7)	1.5864(4)
\vec{M}_c		$M(010)$
\vec{M}_s		$M\left(\frac{-2}{\sqrt{3}} \frac{-1}{\sqrt{3}} 0\right)$
$M(\mu_B)$		6.94(1)
R_{Bragg}	6.07	6.64
$R_{\text{Bragg}}(\text{Mag.})$		1.59

2. Temperature dependence

Figure 5 shows a 2D plot of the thermo-diffractograms obtained at 8 GPa as the system was heated from 5 K to RT. From them, the onset of the helical magnetic ordering is estimated to occur around $T_N = 105(2)$ K, with the appearance of a peak at $d \sim 21$ Å ($2\theta \sim 7^\circ$), which is in agreement with previous studies^{11–13,25}.

The temperature dependence of the intensity for the (101) nuclear reflection (in black) and the satellite $(000) \pm \vec{k}_{\text{HM}}$ (in red) is shown in Fig. 6(b). The evolution of these two lines allows to quantitatively distinguish between the magnetic phases that can be present, as the nuclear and satellite peaks chosen should be the most sensible if a FM ($\vec{k}_{\text{FM}} = (000)$) or HM order (\vec{k}_{HM}), respectively, should be present. No change is observed neither in the (101) nuclear reflection, nor other nuclear lines, as the temperature decreases. This fact supports the hypothesis of absence of any FM ordering, or if present, put an upper limit of $0.2\mu_B$ to such contribution.

Regarding the evolution with temperature of the satellite $(000) \pm \vec{k}_{\text{HM}}$, its intensity was fitted to the power law $I \propto \epsilon^{2\beta}$, where $\epsilon = T_N - T$ is the reduced temperature (see Fig. 7). The obtained value for the critical exponent is $\beta = 0.40(1)$, which is in good agreement with the value predicted by Bak and Mukamel⁴⁸, and reported by previous studies for pure helimagnetic phases at AP and 130 K conditions^{49–52}. It constitutes another indication of the absence of any FM component.

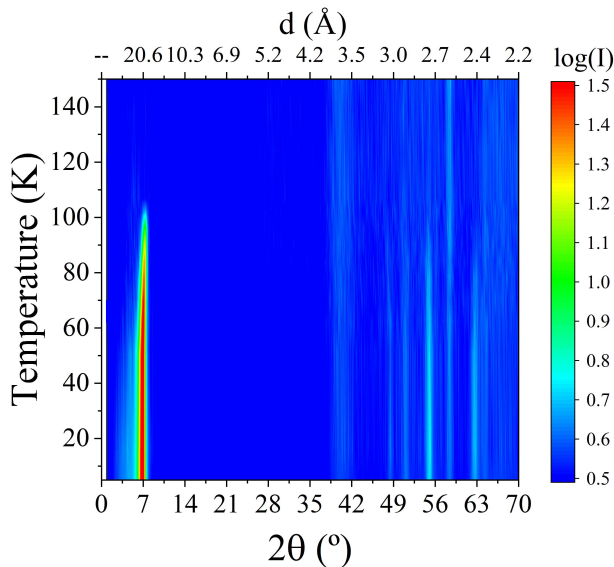


FIG. 5. (Colour online) 2D plot of the thermo-diffractograms measured at 8 GPa with $\lambda = 2.52 \text{ \AA}$ as the system was heated from 5 K to RT. The appearance of the peak at $d \sim 21 \text{ \AA}$ ($2\theta \sim 7^\circ$) is clearly visible at $T = 105(2) \text{ K}$.

Using the magnetic model labelled by the $P6_322.1'(00\gamma)h00s$ MSSG to fit the diffraction patterns collected at each temperature, the dependence of the pitch angle, ϕ , and modulus, M , of the Ho magnetic moment versus temperature was obtained (see Fig. 6(c)).

As the temperature decreases below $T_N \sim 105(2) \text{ K}$, the magnetic moment increases until it saturates at $6.94(1)\mu_B$, a value in good agreement with the saturation magnetization obtained at AP and $T = 5 \text{ K}$ ¹². Meanwhile, the ϕ angle decreases following two linear dependences from $48.6(1)^\circ$ at 105 K to $45.65(2)^\circ$ at 5 K, with a change of slope around $T \sim 40 \text{ K}$. This evolution is also coherent with previous neutron diffraction experiments²⁵, and can be understood if we consider the strong dependence of the helix period with the axial ratio c/a of the hexagonal phase⁸. Such dependence can also explain the change observed around 40 K, since the ratio c/a is stabilized below that temperature (see Fig. 6(a)).

IV. DISCUSSION

In our last study using SQUID magnetization measurements it was reported that the HM order survives up to $P = 12 \text{ GPa}$, while the disappearance of the FM order, or, at least, a remarkable suppression of ferromagnetic net magnetic moments, was observed above 8 GPa¹³. As the intensity of the FM anomaly could not be detected just above the critical pressure for the phase boundary between the *hcp* and Sm-type phases, it was suggested that the disappearance of the FM order is related to the structural phase transition.

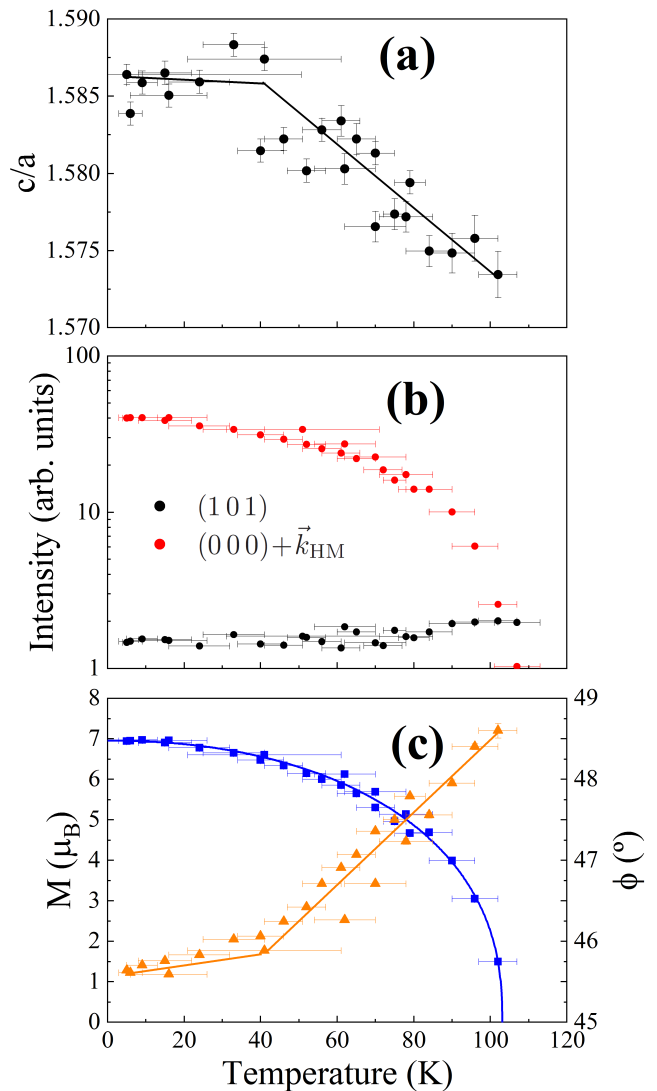


FIG. 6. (Colour online) (a) Temperature dependence of the ratio c/a . (b) Logarithmic scale plot of the intensity evolution with temperature for the nuclear peak (101) (black) and the satellite reflection $(000) \pm \vec{k}_{\text{HM}}$ (red). These peaks are marked with black and red asterisks in the diffractograms of Fig. 3. (c) Temperature dependence of the modulus $M(\mu_B)$ (blue squares) and ϕ angle values (orange triangles). The lines are a guide to the eyes. A change in the linear behaviour of ϕ is observed at around 40 K.

However, the present neutron diffraction experiments, focused on the magnetic structure at $P = 8 \text{ GPa}$, confirm that the *hcp* structure remains stable until at least 8 GPa. Additionally, an incommensurate HM order is observed below $T_N = 105(2) \text{ K}$, which persists down to the lowest temperature measured ($T = 5 \text{ K}$), while no evidence of FM ordering was observed within the entire temperature range. Therefore, the present results help to clarify that the FM order becomes unstable and disappear just before the structural phase transition. Fur-

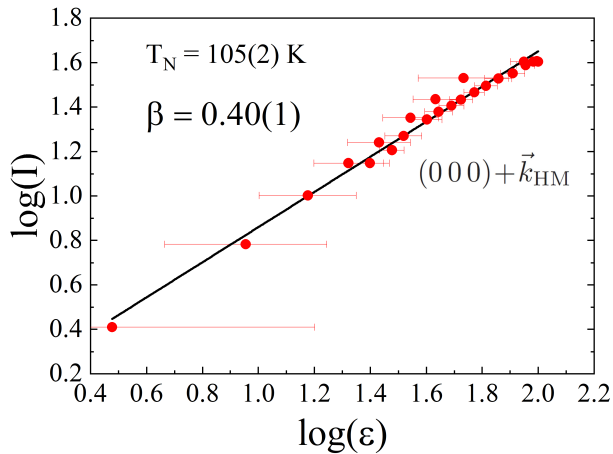


FIG. 7. (Colour online) Logarithmic plot of the intensity of the satellite reflection $(000) \pm \vec{k}_{\text{HM}}$ as a function of the reduced temperature. The value of the transition temperature T_{N} was estimated from Fig. 5.

thermore, the magnetic structure observed at 8 GPa is consistent with previous magnetic measurements, taking into account the pressure distribution with the order of ± 0.5 GPa during the high-pressure experiment.

In the neutron diffraction study by Perreault *et al.*, the FM order was reported to survive in both the Sm-type phase at 14.2 GPa and the *dhcp* phase at 20.2 GPa²⁵. This FM transition was marked by the appearance of a magnetic peak at $d = 3$ Å accompanied by an increase in the intensity of all nuclear peaks. However, in those experiments only a small region of d -spacing (1.0–3.5 Å) was covered, which made it difficult to elucidate the additional existence of HM order at those pressures, since the expected most intense magnetic signal should appear at larger d -spacing (see Fig. 3). Therefore, it would be interesting to confirm these results by performing neutron experiments at such pressures in a long d -spacing diffractometer.

V. CONCLUSION

We conducted neutron diffraction experiments to investigate the magnetic structures of Ho at $P = 8$ GPa. Our findings indicate that the nuclear symmetry remains unchanged, preserving the hexagonal close-packed (*hcp*) symmetry at $P = 8$ GPa. The helimagnetic order persists down to 5 K, and the analysis of its magnetic structure, using the magnetic superspace group formalism, allows to determine the critical exponent $\beta = 0.40(1)$, in agreement with previous theoretical model for pure helices. Meanwhile no FM contribution is observed at any temperature. These results are consistent with previously published findings from magnetization experiments.

ACKNOWLEDGMENTS

This work was supported by Grants-in-Aid for Scientific Research, Grant No. 19KK0070, from the Ministry of Education, Culture, Sports, Science and Technology (MEXT), Japan. The authors acknowledge support by Grants No. PID2022-138492NB-I00-XM4 funded by MCIN/AEI/10.13039.501100011033, OTR02223-SpINS from CSIC/MCIN and DGA/M4 from Diputación General de Aragón (Spain). MPS acknowledges a predoctoral research fellowship from Diputación General de Aragón (Spain). Authors acknowledge the SANE service of ILL and in particular to C. Payre for his valuable support during the experiments.

- ¹S. Chikazumi, *Physics of Ferromagnets* (Oxford Univ. Press., New York, 1997).
- ²E. C. Stoner, “Collective electron ferromagnetism II. Energy and specific heat,” *Proc. Roy. Soc. (London) A* **169**, 339 (1939).
- ³M. Ruderman and C. Kittel, “Indirect exchange coupling of nuclear magnetic moments by conduction electrons,” *Phys. Rev.* **96**, 99 (1954).
- ⁴T. Kasuya, “A theory of metallic ferro- and antiferromagnetism on Zener’s model,” *Prog. Theor. Phys.* **16**, 45–57 (1956).
- ⁵K. Yosida, “Magnetic properties of Cu-Mn alloys,” *Phys. Rev.* **106**, 893 (1957).
- ⁶J. Akella, G. S. Smith, and A. P. Jephcoat, “High-pressure phase transformation studies in gadolinium to 106 GPa,” *J. Phys. Chem. Solids* **49**, 573–576 (1988).
- ⁷W. Grosshans and W. Holzapfel, “Atomic volumes of rare-earth metals under pressures to 40 GPa and above,” *Phys. Rev. B* **45**, 5171 (1992).
- ⁸I. D. Hughes, M. Däne, A. Ernst, W. Hergert, M. Lüders, J. Poulter, J. B. Staunton, A. Svane, Z. Szotek, and W. M. Temmerman, “Lanthanide contraction and magnetism in the heavy rare earth elements,” *Nature* **446**, 650–653 (2007).
- ⁹D. McWhan and A. Stevens, “Effect of pressure on the magnetic properties and crystal structure of Gd, Tb, Dy, and Ho,” *Phys. Rev.* **139**, A682 (1965).
- ¹⁰T. Iwamoto, M. Mito, M. Hitaka, T. Kawae, and K. Takeda, “Magnetic measurement of rare earth ferromagnet gadolinium under high pressure,” *Physica B* **329** (2003).
- ¹¹D. D. Jackson, V. Malba, S. T. Weir, P. A. Baker, and Y. K. Vohra, “High-pressure magnetic susceptibility experiments on the heavy lanthanides Gd, Tb, Dy, Ho, Er, and Tm,” *Phys. Rev. B* **71**, 184416 (2005).
- ¹²M. Mito, K. Matsumoto, Y. Komorida, H. Deguchi, S. Takagi, T. Tajiri, T. Iwamoto, T. Kawae, M. Tokita, and K. Takeda, “Volume shrinkage dependence of ferromagnetic moment in the lanthanide ferromagnets gadolinium, terbium, dysprosium, and holmium,” *J. Phys. Chem. Solids* **70**, 1290–1296 (2009).
- ¹³M. Mito, Y. Kimura, K. Yamakata, M. Ohkuma, H. Chayamichi, T. Tajiri, H. Deguchi, and M. Ishizuka, “Relationship of magnetic ordering and crystal structure in lanthanide ferromagnets Gd, Tb, Dy, and Ho at high pressures,” *Phys. Rev. B* **103**, 24444 (2021).
- ¹⁴S. A. Thomas, W. O. Uhoya, G. M. Tsoi, L. E. Wenger, Y. K. Vohra, G. N. Chesnut, S. T. Weir, C. A. Tulk, and A. M. dos Santos, “Neutron diffraction and electrical transport studies on the incommensurate magnetic phase transition in holmium at high pressures,” *Journal of Physics: Condensed Matter* **24**, 216003 (2012).
- ¹⁵G. K. Samudrala, G. M. Tsoi, S. T. Weir, and Y. K. Vohra, “Structural and magnetic phase transitions in gadolinium under

- high pressures and low temperatures,” *High Pressure Res.* **34**, 385–391 (2014).
- ¹⁶S. A. Thomas, J. M. Montgomery, G. M. Tsoi, Y. K. Vohra, G. N. Chesnut, S. T. Weir, C. A. Tulk, and A. M. dos Santos, “Neutron diffraction and electrical transport studies on magnetic ordering in terbium at high pressures and low temperatures,” *High Pressure Res.* **33**, 555–562 (2013).
- ¹⁷G. K. Samudrala, G. M. Tsoi, S. T. Weir, and Y. K. Vohra, “Magnetic ordering temperatures in rare earth metal dysprosium under ultrahigh pressures,” *High Pressure Res.* **34**, 266–272 (2014).
- ¹⁸J. Lim, G. Fabbri, D. Haskel, and J. S. Schilling, “Magnetic ordering at anomalously high temperatures in Dy at extreme pressures,” *Phys. Rev. B* **91**, 045116 (2015).
- ¹⁹J. Lim, G. Fabbri, D. Haskel, and J. S. Schilling, “Anomalous pressure dependence of magnetic ordering temperature in Tb revealed by resistivity measurements to 141 GPa: Comparison with Gd and Dy,” *Phys. Rev. B* **91**, 174428 (2015).
- ²⁰J. Lim, G. Fabbri, D. Haskel, and J. S. Schilling, “Record high magnetic ordering temperature in a lanthanide at extreme pressure,” *J. Phys: Conference Series* **950**, 042025 (2017).
- ²¹H. Umeyayashi, G. Shirane, B. Frazer, and W. Daniels, “Neutron diffraction study of Tb and Ho under high pressure,” *Phys. Rev.* **165**, 688–692 (1968).
- ²²S. Kawano, N. Achiwah, A. Onodera, and Y. Nakaid, “Neutron diffraction studies of pressure effects on magnetic structures of Tb,” *Physica B* **180** (1992).
- ²³C. Perreault, Y. Vohra, A. dos Santos, J. Molaison, and R. Boehler, “Magnetic ordering in rare earth metal dysprosium revealed by neutron diffraction studies in a large-volume diamond anvil cell,” *High Pressure Res.* **38**, 588–597 (2019).
- ²⁴C. S. Perreault, Y. K. Vohra, A. M. dos Santos, and J. J. Molaison, “Magnetic structure of antiferromagnetic high-pressure phases of dysprosium,” *J. Magn. Magn. Mater.* **545**, 168749 (2022).
- ²⁵C. Perreault, Y. Vohra, A. dos Santos, and J. Molaison, “Neutron diffraction study of magnetic ordering in high pressure phases of rare earth metal holmium,” *J. Magn. Magn. Mater.* **507**, 166843 (2020).
- ²⁶N. C. Cunningham, W. Qiu, and Y. K. Vohra, “Observation of complete regular trivalent rare earth sequence in heavy lanthanide metal holmium under high pressure,” *High Pressure Research* **26**, 43–50 (2006).
- ²⁷W. Bi, E. Alp, J. Song, Y. Deng, J. Zhao, M. Hu, D. Haskel, and J. M. Schilling, *MAR17 Meeting of APS* (<http://meetings.aps.org/link/BAPS.2017.MAR.B35.15>, 2017).
- ²⁸W. C. Koehler, J. W. Cable, M. K. Wilkinson, and E. O. Wollan, “Magnetic structures of Holmium. I. The virgin state,” *Physical Review* **151**, 414–424 (1966).
- ²⁹M. J. Pechan and C. Stassis, “Magnetic structure of holmium,” *Journal of Applied Physics* **55**, 1900–1902 (1984).
- ³⁰J. A. Simpson, D. F. McMorrow, R. A. Cowley, and D. A. Jehan, “Trigonal interactions in holmium,” *Phys. Rev. B* **51**, 16073–16082 (1995).
- ³¹N. Achiwa, S. Kawano, A. Onodera, and Y. Nakai, “Effects of pressure on the helical turn angle of holmium,” *Le Journal de Physique Colloques* **49**, C8–349–C8–350 (1988).
- ³²G. K. Samudrala and Y. K. Vohra, “Structural Properties of Lanthanides at Ultra High Pressure,” in *Handbook on the Physics and Chemistry of Rare Earths*, Vol. 43 (Elsevier, 2013) pp. 275–319.
- ³³A. Janner and T. Janssen, “Symmetry of incommensurate crystal phases. I. Commensurate basic structures,” *Acta Crystallographica Section A* **36**, 399–408 (1980).
- ³⁴J. M. Perez-Mato, J. L. Ribeiro, V. Petricek, and M. I. Aroyo, “Magnetic superspace groups and symmetry constraints in incommensurate magnetic phases,” *Journal of Physics: Condensed Matter* **24**, 163201 (2012).
- ³⁵J. Rodríguez-Carvajal and J. Villain, “Magnetic structures,” *Comptes Rendus Physique* **20**, 770–802 (2019).
- ³⁶J. Besson, R. Nelves, G. Hamel, J. Loveday, G. Weill, and S. Hull, “Neutron powder diffraction above 10 GPa,” *Physica B* **180** (1992).
- ³⁷S. Klotz, T. Strässle, G. Rouse, G. Hamel, and V. Pomjakushin, “Angle-dispersive neutron diffraction under high pressure to 10 GPa,” *Applied Physics Letters* **86**, 031917 (2005).
- ³⁸S. Klotz, T. Hansen, E. Lelièvre-Berna, L. Amand, J. Maurice, and C. Payre, “Advances in the use of Paris-Edinburgh presses for high pressure neutron scattering,” *Journal of Neutron Research* **21**, 117–124 (2020).
- ³⁹J. W. Otto, J. K. Vassiliou, and G. Frommeyer, “Nonhydrostatic compression of elastically anisotropic polycrystals. I. Hydrostatic limits of 4:1 methanol-ethanol and paraffin oil,” *Physical Review B* **57**, 3253–3263 (1998).
- ⁴⁰J. Rodríguez-Carvajal, “Recent advances in magnetic structure determination by neutron powder diffraction,” *Physica B: Condensed Matter* **192**, 55 – 69 (1993).
- ⁴¹H. T. Stokes, D. M. Hatch, and B. J. Campbell, “ISODISTORT, ISOTROPY software suite,” iso.byu.edu (2017).
- ⁴²B. J. Campbell, H. T. Stokes, D. E. Tanner, and D. M. Hatch, “ISODISPLACE: a web-based tool for exploring structural distortions,” *Journal of Applied Crystallography* **39**, 607–614 (2006).
- ⁴³M. I. Aroyo, J. M. Perez-Mato, D. Orobengoa, E. Tasci, G. de la Flor, and A. Kirov, “Crystallography online: Bilbao Crystallographic Server,” *Bulgarian Chemical Communications* **43**, 183–197 (2011).
- ⁴⁴M. I. Aroyo, J. M. Perez-Mato, C. Capillas, E. Kroumova, S. Ivantchev, G. Madariaga, A. Kirov, and H. Wondratschek, “Bilbao Crystallographic Server: I. Databases and crystallographic computing programs,” *Zeitschrift für Kristallographie - Crystalline Materials* **221** (2006), 10.1524/zk
- ⁴⁵M. I. Aroyo, A. Kirov, C. Capillas, J. M. Perez-Mato, and H. Wondratschek, “Bilbao Crystallographic Server. II. Representations of crystallographic point groups and space groups,” *Acta Crystallographica Section A Foundations of Crystallography* **62**, 115–124 (2006).
- ⁴⁶J. Perez-Mato, S. Gallego, E. Tasci, L. Elcoro, G. de la Flor, and M. Aroyo, “Symmetry-based computational tools for magnetic crystallography,” *Annual Review of Materials Research* **45**, 217–248 (2015).
- ⁴⁷We adopted the international notation for the *irreps* labels and MSSG established in^{41–43}.
- ⁴⁸P. Bak and D. Mukamel, “Physical realizations of $n \geq 4$ -component vector models. III. Phase transitions in Cr, Eu, MnS₂, Ho, Dy, and Tb,” *Physical Review B* **13**, 5086–5094 (1976).
- ⁴⁹J. Eckert and G. Shirane, “A neutron diffraction determination of the critical exponent β for the $n = 4$ system holmium,” *Solid State Communications* **19**, 911–912 (1976).
- ⁵⁰T. R. Thurston, G. Helgesen, D. Gibbs, J. P. Hill, B. D. Gaulin, and G. Shirane, “Observation of two length scales in the magnetic critical fluctuations of holmium,” *Physical Review Letters* **70**, 3151–3154 (1993).
- ⁵¹T. R. Thurston, G. Helgesen, J. P. Hill, D. Gibbs, B. D. Gaulin, and P. J. Simpson, “X-ray- and neutron-scattering measurements of two length scales in the magnetic critical fluctuations of holmium,” *Physical Review B* **49**, 15730–15744 (1994).
- ⁵²V. P. Plakhty, W. Schweika, T. Bruckel, J. Kulda, S. V. Gavrilov, L.-P. Regnault, and D. Visser, “Chiral criticality in helimagnet Ho studied by polarized neutron scattering,” *Physical Review B* **64** (2001).